This article has been accepted for publication in a future issue of this journal, but has not been fully edited. Content may change prior to final publication. Citation information: DOI 10.1109/TCOMM.2018.2854164, IEEE Transactions on Communications

Dual-polarized Faster-than-Nyquist Transmission Using Higher-order Modulation Schemes

Mrinmoy Jana, Lutz Lampe and Jeebak Mitra

***Abstract*—Faster-than-Nyquist (FTN) transmission employing antenna polarization multiplexing and higher-order modulation (HoM) schemes can significantly increase the spectral efficiency (SE) of the existing wireless backhaul links. However, the benefits of each of these SE enhancement techniques come with a price. While FTN introduces inter-symbol interference (ISI), a dual-polarized (DP) transmission suffers from cross-polarization interference (XPI) and HoM makes a communication system vulnerable to phase-noise (PN) distortions. In this paper, we investigate for the first time a DP-FTN HoM transmission system. We propose a cross-polarization interference cancellation (XPIC) and PN mitigation structure, coupled with adaptive decision-feedback equalization or linear precoding, to jointly mitigate interference and accomplish carrier-phase tracking. The DP systems combined with the FTN signaling presented in this paper offer more than 150% increase in SE compared to a single-polarized (SP) Nyquist transmission. The effectiveness of the proposed algorithms is demonstrated through computer simulations of a coded DP-FTN microwave communication system in the presence of PN. Numerical results suggest that with the proposed interference cancellation methods, a DP-FTN transmission can yield a $3-5.5$ dB performance improvement over an equivalent DP-Nyquist system that employs a higher modulation order to achieve the same data rate.**

***Index Terms*—Faster-than-Nyquist (FTN) transmission, cross-polarization interference cancellation (XPIC), dual polarization (DP), phase noise (PN), inter-symbol interference (ISI), pre-equalization, precoding, decision-feedback equalization (DFE), higher-order-modulation (HoM), microwave backhaul.**

I. Introduction

RAPIDLY growing demands for next-generation cellular data rates warrant adopting new means to increase the spectral efficiency (SE) of the fixed wireless backhaul links, where line-of-sight and point-to-point microwave radio systems are widely used due to their fast and cost-effective deployment. One way to accomplish this SE improvement is to employ Faster-than-Nyquist (FTN) transmission [2]–[7], which deliberately relinquishes the time-frequency spacing requirements of adjacent symbols imposed by the Nyquist criterion. By giving up this orthogonality condition, theoretically, FTN signaling provides a higher achievable rate [8]. Moreover, to further the SE improvement of a microwave radio, FTN can be combined with antenna polarization multiplexing and higher-order modulation (HoM) schemes. While adopting HoM for such microwave systems is a very well-known technique, dual-polarized (DP) transmission has also attracted a considerable attention in the past few years [9]–[19]. An ideal DP transmission system, where two data-streams are transmitted at the same carrier frequency by two orthogonal polarizations, i.e. the horizontal (H) and the vertical (V) polarization, offers a doubling of the data rate compared to a single-polarized (SP) transmission. However, FTN introduces inter-symbol interference (ISI) and DP transmission suffers from cross-talk between the two polarization branches, known as cross-polarization interference (XPI). Furthermore, adopting HoM makes the communication system sensitive to phase noise (PN) distortions that arise due to imperfections in the transmitter and receiver local oscillators (LOs). Therefore, in order to fully afford the SE benefits a DP-FTN HoM transmission offers, efficient mitigation techniques are required to counter these detrimental effects. The effectiveness of the equalization and PN compensation schemes is particularly crucial when forward-error correcting (FEC) codes are employed, which operate in the low to moderate signal-to-noise ratio (SNR) regime.

This work was supported by the Natural Sciences and Engineering Research Council of Canada (NSERC) and Huawei Technologies, Canada.

Part of this work was presented at the 19th IEEE Int. Workshop on Sig. Proc. Adv. in Wireless Commun. (SPAWC), Kalamata, Greece, June 2018 [1].

Mrinmoy Jana, and Lutz Lampe are with the Department of Electrical and Computer Engineering, University of British Columbia, BC, Canada. Email: mjana@ece.ubc.ca, lampe@ece.ubc.ca. Jeebak Mitra is with Huawei Technologies, Ottawa, Canada. Email: jeebak.mitra@huawei.com.

A. State-of-the-Art in XPIC, FTN and PN Mitigation

DP systems employing cross-polarization interference cancellation (XPIC) at the receiver have been well investigated in the microwave communication literature for a Nyquist transmission in the context of "synchronous" [9]–[16] and "asynchronous" [17]–[19] transmissions. In a synchronous DP transmission, time and frequency-synchronized received samples from both polarization branches are processed by a two-dimensional (2-D) XPIC filter to remove cross-talk between the two orthogonal polarizations. Alternatively, in an asynchronous transmission, absence of knowledge about the transmission parameters of the respective other polarization branch precludes the feasibility of performing synchronization on the interfering data stream. However, the algorithms in previous works for these systems do not consider some of the practical challenges encountered in a microwave radio system. For example, [9]–[16] describe the XPI mitigation techniques without furnishing sufficient details about the PN compensation algorithms. On the other hand, [17]–[19] present XPIC algorithms together with PN mitigation approaches, assuming an additive white Gaussian noise (AWGN) channel and perfect knowledge of the XPI channel at the receiver. In practice, a microwave channel can introduce slowly time-varying ISI due to multipath effects [12], [14], [20] and the availability of a perfect estimate of the XPI channel at the

This article has been accepted for publication in a future issue of this journal, but has not been fully edited. Content may change prior to final publication. Citation information: DOI 10.1109/TCOMM.2018.2854164, IEEE Transactions on Communications

receiver is somewhat unrealistic, particularly in the presence of PN [21]. Moreover, none of the above works considers additional ISI induced by an FTN transmission.

Combining FTN signaling with a DP transmission is motivated by the following two benefits: (a) FTN signaling can further the SE improvement a DP system provides, e.g. using an FTN acceleration factor of 0.8 for the two orthogonal data streams offers a 150% increase in SE compared to an SP Nyquist transmission, and (b) for a target data rate, FTN transmission can moderate the need for very high modulation orders that are more vulnerable to PN distortions, especially in a DP transmission, where phase impairments originating in the transmitter LO of one orthogonal polarization can affect the demodulation performance of the other due to cross-talk between the polarization branches. Under these circumstances, a DP-FTN transmission, with efficient interference mitigation techniques, can yield a significant SNR advantage over a DP-Nyquist system that employs a higher modulation order to achieve the same data rate. Enjoying the above benefits of FTN signaling entails successful equalization of the FTN-induced ISI. For this, a significant volume of work considers Bahl-Cocke-Jelinek-Raviv (BCJR) based maximum a-posteriori probability (MAP) equalization [22]–[25]. However, it is difficult to apply these methods to a DP-FTN HoM system primarily because their computational complexity becomes intractable as the number of BCJR states increases significantly for very high modulation orders. There is also another body of works [26]–[31] that can be applied to higher modulation formats without significant increase in complexity. However, they employ computationally prohibitive and buffer-space constrained iterative equalization schemes, and require explicit channel estimation, which is not computationally trivial in the presence of PN [21], [32]. Moreover, the above works do not consider any PN mitigation schemes.

Practical microwave systems for spectrally efficient transmission are evolving towards adopting very high modulation orders, e.g. 4096-QAM [33], that need robust PN compensation techniques. In light of that, we note the factor-graph based methods for joint FTN and PN mitigation [34], [35], and also the block-based iterative PN compensation techniques [36], [37] in an SP transmission under an AWGN channel. However, the above methods would require additional estimation and equalization algorithms for the unknown co-polarization and cross-polarization ISI channels in a DP transmission. The extension of the above mentioned algorithms to a DP-FTN HoM transmission under consideration is not straight-forward because channel estimation, FTN and multi-path ISI equalization, and PN compensation tasks are not modular, which invites a joint mitigation approach [21], [32]. Therefore, combining the individual solutions is challenging under these circumstances, which warrants considerable research, and can be subject to future work. In this work, we consider a 2-D adaptive decision feedback equalizer (DFE) to jointly mitigate interference and accomplish carrier phase recovery in a DP-FTN transmission. We note that 2-D DFE structures without carrier phase recovery have been well studied in the context of multiple-input multiple-output (MIMO) transmission [38]–[40], and that previous works on combining DFE with carrier phase recovery have focused on transmissions with a single polarization [41]–[43]. In the following, we highlight the contribution of our work in more detail.

B. Contributions and Outline

This paper is the first to present a synchronous DP-FTN HoM system with the objective to increase the data rate of the existing microwave links. Therefore, we assume that timing and frequency synchronization of both polarization data streams are performed prior to the receiver signal processing. To provide a solution for spectrally efficient microwave transmissions with practical impairments, the present work addresses a number of challenges in the form of XPIC in a DP transmission without the explicit knowledge of the interference channel, FTN and multi-path ISI equalization, and carrier phase tracking. For this purpose, we propose a simple non-iterative approach, as opposed to computationally demanding iterative equalization schemes. This makes our solution scalable to very high modulation orders, and adaptive to channel variations. The proposed adaptive approach also works efficiently even in the absence of XPI, corresponding to an SP transmission scenario. The primary challenge to devise a practical adaptive interference mitigation scheme lies in designing the pilot symbols required for the training-based equalization due to corruption of the clean constellation symbols by FTN-induced ISI. To counter this, two possible solutions can be adopted, i.e. either (a) combine the FTN-ISI with the multi-path ISI/XPI, or (b) pre-compensate for the FTN-ISI so that clean pilots can be used to equalize the residual multi-path ISI/XPI. For the approach (a) above, the overall interference cancellation problem can be formulated as a DP-Nyquist transmission, together with XPIC and PN mitigation for the two polarization branches. As our *first* contribution, we extend the DFE-based receiver structures from [41], [42] to the DP system of interest. To this end, we derive an adaptive estimator for the aggregate PN, stemming from the transmitter and receiver LOs. However, in the presence of a significant cross-talk between the two polarizations, PN generated at the transmitter LO of one orthogonal polarization can significantly influence the demodulation performance of the other. Motivated by this, as our *second* contribution, we propose an adaptive technique to track the transmitter and receiver phase noise processes separately for both orthogonal polarizations. The performance gains offered by the second method over the first, however, come at a price of slightly more computations and storage requirements. Further, exploiting the fact that the ISI induced by FTN is known at the transmitter, approach (b) mentioned above can also be applied to facilitate effective elimination of the residual FTN-ISI. Therefore, as our *third* contribution, we extend the linear pre-equalization (LPE) strategy from [44] to the DP-FTN system. Different from [44], the LPE in this paper is used in association with the adaptive DFE coupled with PN tracking, to form a combined equalization and PN mitigation structure. Numerical results in Section V-C of our paper advocates promising performance gains of this combined structure over a DFE-only equalization approach.

This article has been accepted for publication in a future issue of this journal, but has not been fully edited. Content may change prior to final publication. Citation information: DOI 10.1109/TCOMM.2018.2854164, IEEE Transactions on Communications

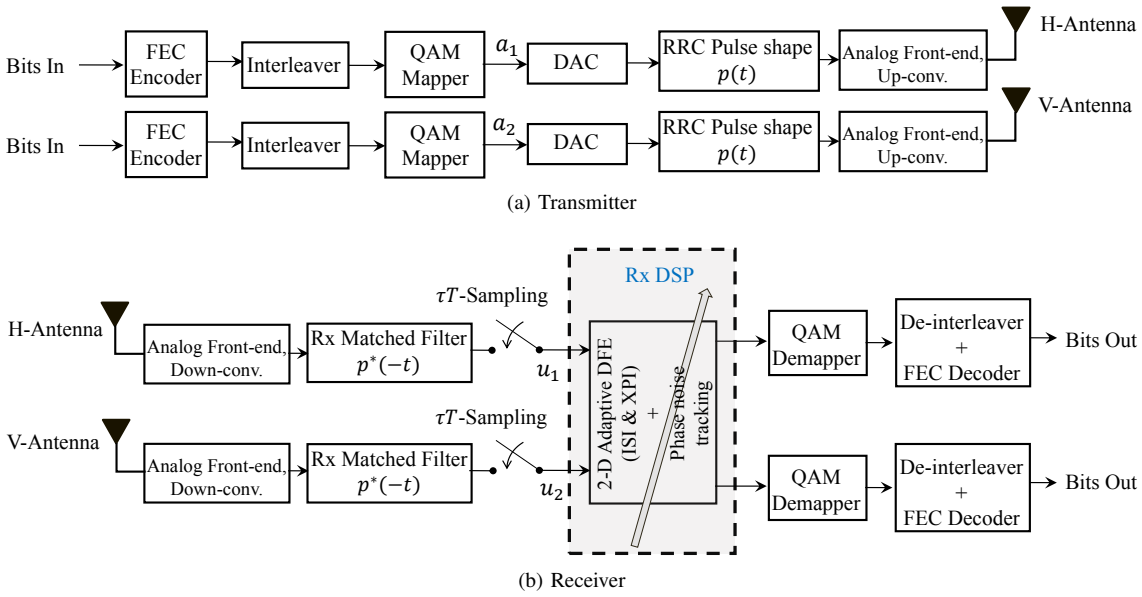

Fig. 1. System model for a DP-FTN transmission.

TABLE I
TABLE OF ACRONYMS

Acronym	Definition
BER	Bit Error Rate
CPNT	Combined Phase noise Tracking
DFE	Decision Feedback Equalizer
DP	Dual Polarization
FBF	Feedback Filter
FEC	Forward Error Correction
FFF	Feed-forward Filter
FTN	Faster-than Nyquist
HoM	Higher-order Modulation
IPNT	Individual Phase noise Tracking
ISI	Inter-symbol Interference
LMS	Least Mean-square
LPE	Linear Pre-equalization
MSE	Mean-square Error
PAPR	Peak-to-average Power Ratio
PN	Phase noise
QAM	Quadrature Amplitude Modulation
RRC	Root-Raised-Cosine
SE	Spectral Efficiency
SNR	Signal-to-noise Ratio
SP	Single-polarized
XPD	Cross-polarization Discrimination
XPI	Cross-polarization Interference
XPIC	Cross-polarization Interference Cancellation

The remainder of the paper is organized as follows. The system model is introduced in Section II. In Section III, we propose two new adaptive DFE-based equalization schemes to jointly mitigate ISI, XPI and PN. The pre-equalized FTN transmission along with XPIC and PN cancellation is presented for a DP-FTN system in Section IV. Section V demonstrates the benefits of our proposals through simulations. Finally, Section VI provides concluding remarks.

For clarity of notation usage, Table I lists the frequently used acronyms and their corresponding definitions.

II. System Model

We consider the transmitter and receiver of a DP-FTN microwave system shown in Fig. 1. As depicted in the transmitter of Fig. 1(a), the input data bits for the H and V polarizations are first FEC encoded and interleaved, followed by quadrature amplitude modulation (QAM). The modulated data streams a_1 and a_2 are then pulse-shaped by T-orthogonal pulses p, converted into analog signals, up-converted to a microwave carrier frequency and then transmitted with an FTN acceleration factor $\tau < 1$ on H and V-polarizations, respectively. The resulting transmitted analog signals for the H and V streams can be written as

$$s_1(t) = \mathrm{Re}\Big\{ \mathrm{e}^{\mathrm{j}\left(2\pi f_c t + \vartheta_{t_1}(t)\right)} \sum_k a_1[k] p(t - k\tau T) \Big\}, \quad (1)$$

$$s_2(t) = \mathrm{Re}\Big\{ \mathrm{e}^{\mathrm{j}\left(2\pi f_c t + \vartheta_{t_2}(t)\right)} \sum_k a_2[k] p(t - k\tau T) \Big\}, \quad (2)$$

where f_c is the carrier frequency, ϑ_{t_1} and ϑ_{t_2} are the phase noise impairments, associated with the H and V-transmitter LOs, respectively. For the application of interest, we assume a root-raised-cosine (RRC) pulse-shaping filter p with a roll-off factor β.

The transmitted signals on both polarizations propagate through a wireless channel to reach the DP-FTN receiver shown in Fig. 1(b). At the receiver, the matched-filtered and sampled signals u_1 and u_2 on H and V polarizations, respectively, are processed by a receiver discrete signal processing (Rx-DSP) unit, comprising of an adaptive 2-D equalizer and PN tracker, as detailed in Section III. Thereafter, the recovered H and V polarization signals are demodulated and FEC-decoded to produce the output bits.

The equivalent discrete-time baseband model for the DP-FTN system is demonstrated in Fig. 2, where the received

This article has been accepted for publication in a future issue of this journal, but has not been fully edited. Content may change prior to final publication. Citation information: DOI 10.1109/TCOMM.2018.2854164, IEEE Transactions on Communications

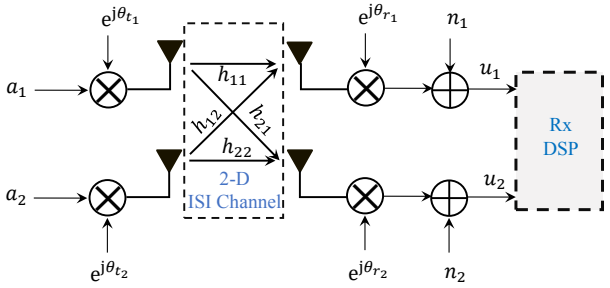

Fig. 2. Equivalent discrete-time baseband system model for a DP-FTN transmission.

samples $u_i[k]$ at a time instant k, with $i = 1, 2$ for H and V polarization, respectively, can be represented as

$$u_i[k] = \mathrm{e}^{\mathrm{j}\theta_{r_i}[k]} \sum_{j=1}^{2} \sum_{l} a_j[k-l] \mathrm{e}^{\mathrm{j}\theta_{t_j}[k-l]} h_{ij}[l] + n_i[k] \,. \quad (3)$$

In (3), $\{h_{ij}\}$ for $i, j \in \{1, 2\}$ denote the effective co-polarization and cross-polarization channel taps, representing the combined effects of the multipath ISI, FTN-ISI and XPI, n_i is a zero-mean additive colored (due to FTN-sampling) Gaussian noise sample with variance $\sigma^2_{n_i}$, and θ_{t_i} and θ_{r_i} represent the sampled transmitter and receiver PN processes, respectively. For the application of interest, the PN processes are assumed to be slowly time-varying [17], [19], [41] and can be modeled by Wiener processes [45] as

$$\theta_{t_i}[k] = \theta_{t_i}[k-1] + w_{t_i}[k] \,, \quad (4)$$
$$\theta_{r_i}[k] = \theta_{r_i}[k-1] + w_{r_i}[k] \,, \quad (5)$$

where w_{t_i} and w_{r_i} are the samples of independent zero-mean Gaussian random variables with variances $\sigma^2_{w_{t_i}}$ and $\sigma^2_{w_{r_i}}$, respectively.

The equivalent baseband system shown in Fig. 2 models the transmitter and receiver PN processes separately, similar to [9]–[11]. For an SP transmission in an AWGN channel, we note that the transmitter and receiver PN processes can be combined to model an equivalent sum PN process [36], [37], [46], [47]. Alternatively, when there is a multi-path channel between the transmitter and the receiver, each received symbol includes the contributions from multiple transmitter PN samples due to ISI [43]. We note that for an SP transmission, combining the transmitter and receiver PN distortions can still be considered to be a good approximation of the true system model for relatively slow time-variation of the PN processes with respect to the ISI duration. However, for DP systems, it is important to characterize all four transmitter and receiver PN processes separately [9]–[11] to model the impact of the cross-polarization transmitter PNs. The numerical results presented in Section V-B of this paper, corresponding to two different PN tracking schemes, stand to further justify such modeling.

With the system model (3) at hand, we now proceed to present two new adaptive equalization and joint PN mitigation techniques in the next section, followed by the precoded DP-FTN transmission strategy in Section IV.

III. Adaptive DFE with PN Compensation

In this section, we present an adaptive DFE approach to jointly optimize the PN estimates and equalizer tap coefficients to mitigate the effects of the two-dimensional interference channel and phase noise processes as illustrated in Fig. 2. We exploit digital data sharing between the two orthogonal polarizations as in [48], which enables us to use the past symbol-decisions from both polarization branches in a feedback loop. With the assumption of a slow time-variation of the transmitter and receiver PN processes [17], [19], [41], the exact knowledge of the PN statistics are not required for the proposed algorithms.

Moreover, the adaptive equalization approach eliminates the need for an explicit channel estimation at the receivers, and the proposed methods do not require iterations[1] between the equalizer and the FEC decoder. The main reasons to not consider iterative decoding and demodulation/equalization in the present work are: (a) the complexity associated with iterative solutions in terms of computations and buffer space, (b) the simpler scalability with very high modulation orders and adaptivity with respect to channel variations of non-iterative and thus non-block-based solutions [9], [11], [12], [41], [46], [49].

A. DFE with Combined Phase Noise Tracking (CPNT)

The concept of joint equalization and carrier phase recovery presented in [41], [49] for an SP system is extended to the DP-FTN transmission in the following and will be referred to as the DFE-CPNT method henceforth.

Fig. 3 shows the Rx-DSP module from Fig. 1(b) in more detail. The received H and V polarization sequences u_1 and u_2 are first de-rotated by the respective PN estimates $\hat{\varphi}_1$ and $\hat{\varphi}_2$, and then fed into an adaptive 2-D DFE. The joint estimation method for the PN processes and the DFE filters are detailed later in this section. Each entry of the feed-forward-filter (FFF) $\boldsymbol{F}$ and the feedback-filter (FBF) $\boldsymbol{B}$ has N_f and N_b taps, respectively. The DFE output sequences y_1 and y_2 are provided as inputs to the soft demappers and FEC decoders. The symbols $y_i[k]$, $i \in \{1, 2\}$, at the k^{th} symbol interval can be written as

$$y_i[k] = \sum_{j=1}^{2} \Bigg(\sum_{\nu=0}^{N_\mathrm{f}-1} f_{ij}[\nu, k] u_j[k-\nu] \mathrm{e}^{-\mathrm{j}\hat{\varphi}_j[k-\nu]} - \sum_{\mu=1}^{N_\mathrm{b}} b_{ij}[\mu, k] \hat{a}_j[k-k_0-\mu] \Bigg) , \quad (6)$$

where $f_{ij}[\nu, k]$ and $b_{ij}[\mu, k]$ denote the ν^{th} and μ^{th} tap at the k^{th} symbol interval corresponding to the i^{th}-row and j^{th}-column entries of $\boldsymbol{F}$ and $\boldsymbol{B}$, respectively, $\hat{a}_1$ and $\hat{a}_2$ are the previous symbol-decisions for the H and V-polarization, respectively, and k_0 denotes the DFE decision delay [38], [50].

[1]This is not to stipulate that iterative solutions may not have merit for dealing with the considered problem, but we argue that it is meaningful to start with computationally simpler and, as our results in Section V show, effective non-iterative solutions. What further gains could be achieved with iterative methods, and under what computational costs and other requirements e.g. with regard to channel variability, can be subject to future work.

This article has been accepted for publication in a future issue of this journal, but has not been fully edited. Content may change prior to final publication. Citation information: DOI 10.1109/TCOMM.2018.2854164, IEEE Transactions on Communications

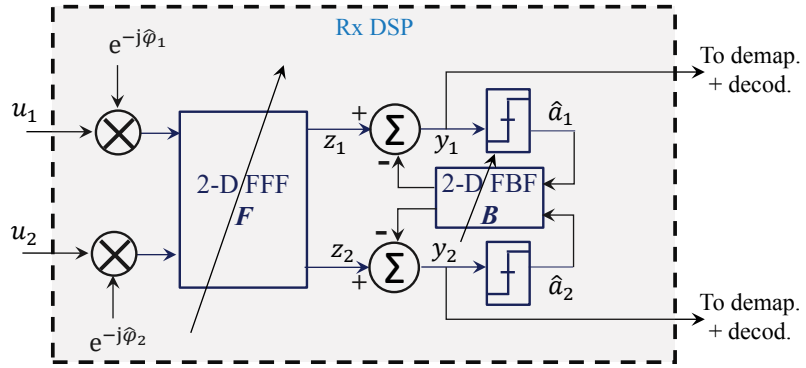

Fig. 3. Detailed Rx-DSP block diagram for the adaptive XPIC and DFE-FTN equalization with CPNT.

For jointly updating the DFE tap-weights and the PN estimates, we use the adaptive least-mean-square (LMS) method [41], [51]. Assuming a slow variation of the PN processes and hence, the PN estimates $\hat{\varphi}_i$ to be practically constant over the duration of N_f symbols corresponding to the FFF length [41], the update algorithms for the 2-D XPIC and PN estimates are dictated by the following lemma.

Lemma 1. *The LMS update equations, computed by the stochastic gradient descent algorithm [51], for the 2-D equalizer tap weights and CPNT estimates are given as*

$$\boldsymbol{f}_1[k+1] = \boldsymbol{f}_1[k] - \alpha \boldsymbol{P}[k]\, \boldsymbol{u}_\mathrm{g}[k] \mathcal{E}_1^*[k]\,, \tag{7}$$

$$\boldsymbol{f}_2[k+1] = \boldsymbol{f}_2[k] - \alpha \boldsymbol{P}[k]\, \boldsymbol{u}_\mathrm{g}[k] \mathcal{E}_2^*[k]\,, \tag{8}$$

$$\boldsymbol{b}_1[k+1] = \boldsymbol{b}_1[k] + \delta \hat{\boldsymbol{a}}_\mathrm{g}[k] \mathcal{E}_1^*[k]\,, \tag{9}$$

$$\boldsymbol{b}_2[k+1] = \boldsymbol{b}_2[k] + \delta \hat{\boldsymbol{a}}_\mathrm{g}[k] \mathcal{E}_2^*[k]\,, \tag{10}$$

$$\hat{\varphi}_1[k+1] = \hat{\varphi}_1[k] - \gamma \Upsilon_1[k]\,, \tag{11}$$

$$\hat{\varphi}_2[k+1] = \hat{\varphi}_2[k] - \gamma \Upsilon_2[k]\,, \tag{12}$$

where for $i \in \{1,2\}$, $\mathcal{E}_i[k] = y_i[k] - \hat{a}_i[k-k_0]$ *are the error signals,* $\alpha > 0$, $\delta > 0$, $\gamma > 0$ *are the LMS step-size parameters and*

$$\boldsymbol{f}_i[k] = \Big[\Big\{ f_{i1}^*[m,k] \Big\}_{m=0}^{N_\mathrm{f}-1}, \Big\{ f_{i2}^*[n,k] \Big\}_{n=0}^{N_\mathrm{f}-1} \Big]^\mathrm{T}, \tag{13}$$

$$\boldsymbol{b}_i[k] = \Big[\Big\{ b_{i1}^*[m,k] \Big\}_{m=1}^{N_\mathrm{b}}, \Big\{ b_{i2}^*[n,k] \Big\}_{n=1}^{N_\mathrm{b}} \Big]^\mathrm{T}, \tag{14}$$

$$\boldsymbol{u}_\mathrm{g}[k] = \Big[\Big\{ u_1[k-m] \Big\}_{m=0}^{N_\mathrm{f}-1}, \Big\{ u_2[k-n] \Big\}_{n=0}^{N_\mathrm{f}-1} \Big]^\mathrm{T}, \tag{15}$$

$$\hat{\boldsymbol{a}}_\mathrm{g}[k] = \Big[\Big\{ \hat{a}_1[k-k_0-m] \Big\}_{m=1}^{N_\mathrm{b}}, \Big\{ \hat{a}_2[k-k_0-n] \Big\}_{n=1}^{N_\mathrm{b}} \Big]^\mathrm{T}, \tag{16}$$

$$\boldsymbol{P}[k] = \mathrm{diag}\Big(\underbrace{e^{-j\hat{\varphi}_1[k]}, \ldots, e^{-j\hat{\varphi}_1[k]}}_{N_\mathrm{f}}, \underbrace{e^{-j\hat{\varphi}_2[k]}, \ldots, e^{-j\hat{\varphi}_2[k]}}_{N_\mathrm{f}} \Big), \tag{17}$$

$$\Upsilon_i[k] = \cos\left(\hat{\varphi}_i[k]\right) \mathrm{Im}(\psi_i[k]) - \sin\left(\hat{\varphi}_i[k]\right) \mathrm{Re}(\psi_i[k])\,, \tag{18}$$

$$\psi_i[k] = \boldsymbol{f}_{1i}^\mathrm{H}[k] \boldsymbol{u}_i[k] \mathcal{E}_1^*[k] + \boldsymbol{f}_{2i}^\mathrm{H}[k] \boldsymbol{u}_i[k] \mathcal{E}_2^*[k] \tag{19}$$

$$\boldsymbol{u}_i[k] = \Big[u_i[k], \ldots, u_i[k-N_\mathrm{f}+1] \Big]^\mathrm{T}, \tag{20}$$

$$\boldsymbol{f}_{ij}[k] = \Big[f_{ij}^*[0,k], \ldots, f_{ij}^*[N_\mathrm{f}-1,k] \Big]^\mathrm{T}, \tag{21}$$

where $(\cdot)^*$, $\mathrm{Re}(\cdot)$, $\mathrm{Im}(\cdot)$ *represent, respectively, the complex conjugate, real and imaginary part of a complex scalar,* $[\cdot]^\mathrm{H}$ *and* $[\cdot]^\mathrm{T}$ *denote the matrix hermitian and transpose, respectively,* $\mathrm{diag}(\cdot)$ *is the diagonal matrix formed with the elements of a vector and the expression* $\{x[j]\}_{j=N_1}^{N_2}$ *denotes the row-vector* $[x[N_1], \ldots, x[N_2]]$.

Proof: See Appendix A. ■

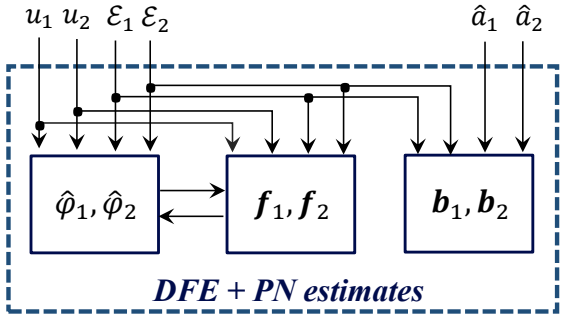

Fig. 4. Joint estimation of the filter tap-weights and PN processes for the DFE-CPNT method.

Fig. 4 shows the schematics of estimating the DFE tap-weights and PN processes for the DFE-CPNT method, by using the symbols u_i, $\hat{a}_i$ and $\mathcal{E}_i$, $i \in \{1,2\}$, according to (7)-(12) of Lemma 1. As can be seen from the figure and the above lemma, the estimation of the DFE-FFF and the PN processes are coupled together, similar to the joint estimation approach adopted in [41], [49]. Additionally, the DFE-CPNT scheme uses the symbol decisions to adapt the equalizer filter coefficients and PN estimates. However, insertion of known pilot symbols at regular intervals [41], [46] for both orthogonal polarization transmissions is required for LMS convergence, particularly when FEC codes are employed which facilitate lower operating SNRs. Hence, the LMS adaptation for the DFE-CPNT method operates in training mode when known pilot symbols are transmitted and switches to a decision-directed mode otherwise. The pilot-symbols density is chosen to meet a desired trade-off between performance and transmission overhead.

Due to the cross-talk between the two orthogonal polarizations in a DP system shown in Fig. 2, the CPNT phase estimate $\hat{\varphi}_1$ in (11) for the H-polarization branch attempts to track the combined PN processes originating in the LOs of the H-polarization transmitter-receiver pair and the V-polarization transmitter. Consequently, the accuracy of the PN estimates depends on the level of XPI and hence, on the

This article has been accepted for publication in a future issue of this journal, but has not been fully edited. Content may change prior to final publication. Citation information: DOI 10.1109/TCOMM.2018.2854164, IEEE Transactions on Communications

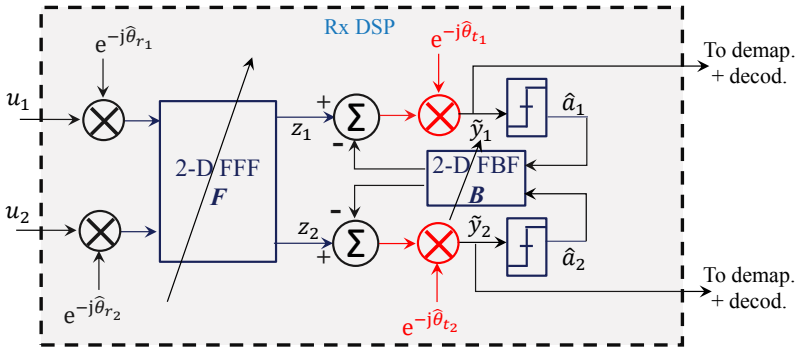

Fig. 5. Detailed Rx-DSP block diagram for the adaptive XPIC and DFE-FTN equalization with IPNT.

cancellation performance of the DFE-based XPIC illustrated in Fig. 3. Therefore, the overall performance can be improved by reducing the interdependence between the PN estimation and XPIC. To this end, we present a second joint equalization and PN tracking method in the following.

B. DFE with Individual Phase Noise Tracking (IPNT)

The DFE with IPNT method estimates the transmitter and receiver PNs of each polarization separately. The detailed block diagram is shown in Fig. 5, where the de-rotation of the filtered signal before the slicer-stage of the DFE is highlighted. This requires tracking of two additional PN processes compared to the CPNT method. The receiver and transmitter PN estimates for the i^{th} polarization branch, for $i \in \{1,2\}$, are denoted by $\hat{\theta}_{r_i}$ and $\hat{\theta}_{t_i}$, respectively. Following the 2-D FFF-FBF filtering and phase compensation, the sequences $\tilde{y}_i$, $i=1,2$, are passed to the FEC decoding. At the k^{th} time instant, $\tilde{y}_i[k]$, $i\in\{1,2\}$, can be written as

$$\tilde{y}_i[k]=\mathrm{e}^{-\mathrm{j}\hat{\theta}_{t_i}[k]}\Bigg(\sum_{j=1}^{2}\Bigg\{\sum_{\nu=0}^{N_\mathrm{f}-1} f_{ij}[\nu,k]u_j[k-\nu]\mathrm{e}^{-\mathrm{j}\hat{\theta}_{r_j}[k-\nu]} - \sum_{\mu=1}^{N_\mathrm{b}} b_{ij}[\mu,k]\hat{a}_j[k-k_0-\mu]\Bigg\}\Bigg). \quad (22)$$

Assuming a slow variation of the PN processes as in Section III-A, the LMS tracking algorithms for the equalizer and the four PN estimates are given in the following lemma.

Lemma 2. *The LMS update equations for equalizer tap weights and PN estimates for the IPNT method are given by*

$$\boldsymbol{f}_1[k+1]=\boldsymbol{f}_1[k]-\tilde{\alpha}\mathrm{e}^{-\mathrm{j}\hat{\theta}_{t_1}[k]}\tilde{\boldsymbol{P}}[k]\,\boldsymbol{u}_\mathrm{g}[k]\mathcal{E}_1^*[k]\,, \quad (23)$$

$$\boldsymbol{f}_2[k+1]=\boldsymbol{f}_2[k]-\tilde{\alpha}\mathrm{e}^{-\mathrm{j}\hat{\theta}_{t_2}[k]}\tilde{\boldsymbol{P}}[k]\,\boldsymbol{u}_\mathrm{g}[k]\mathcal{E}_2^*[k]\,, \quad (24)$$

$$\boldsymbol{b}_1[k+1]=\boldsymbol{b}_1[k]+\tilde{\delta}\mathrm{e}^{-\mathrm{j}\hat{\theta}_{t_1}[k]}\hat{\boldsymbol{a}}_\mathrm{g}[k]\mathcal{E}_1^*[k]\,, \quad (25)$$

$$\boldsymbol{b}_2[k+1]=\boldsymbol{b}_2[k]+\tilde{\delta}\mathrm{e}^{-\mathrm{j}\hat{\theta}_{t_2}[k]}\hat{\boldsymbol{a}}_\mathrm{g}[k]\mathcal{E}_2^*[k]\,, \quad (26)$$

$$\hat{\theta}_{t_1}[k+1]=\hat{\theta}_{t_1}[k]-\tilde{\gamma}_t\Gamma_{t_1}[k]\,, \quad (27)$$

$$\hat{\theta}_{t_2}[k+1]=\hat{\theta}_{t_2}[k]-\tilde{\gamma}_t\Gamma_{t_2}[k]\,, \quad (28)$$

$$\hat{\theta}_{r_1}[k+1]=\hat{\theta}_{r_1}[k]-\tilde{\gamma}_r\Gamma_{r_1}[k]\,, \quad (29)$$

$$\hat{\theta}_{r_2}[k+1]=\hat{\theta}_{r_2}[k]-\tilde{\gamma}_r\Gamma_{r_2}[k]\,, \quad (30)$$

where $\tilde{\alpha}>0$, $\tilde{\delta}>0$, $\tilde{\gamma}_t>0$, $\tilde{\gamma}_r>0$ are the LMS step-size parameters, the remaining variables for $i\in\{1,2\}$ are defined as in Lemma 1 and as below:

$$\tilde{\boldsymbol{P}}[k]=\mathrm{diag}\Big(\underbrace{\mathrm{e}^{-\mathrm{j}\hat{\theta}_{r_1}[k]},\ldots,\mathrm{e}^{-\mathrm{j}\hat{\theta}_{r_1}[k]}}_{N_\mathrm{f}},\underbrace{\mathrm{e}^{-\mathrm{j}\hat{\theta}_{r_2}[k]},\ldots,\mathrm{e}^{-\mathrm{j}\hat{\theta}_{r_2}[k]}}_{N_\mathrm{f}}\Big), \quad (31)$$

$$\Gamma_{t_i}[k]=\cos\Big(\hat{\theta}_{t_i}[k]\Big)\,\mathrm{Im}\left(\xi_i[k]\right)-\sin\Big(\hat{\theta}_{t_i}[k]\Big)\,\mathrm{Re}\left(\xi_i[k]\right), \quad (32)$$

$$\xi_i[k]=\Big(\boldsymbol{f}_i^\mathrm{H}[k]\,\tilde{\boldsymbol{P}}[k]\,\boldsymbol{u}_\mathrm{g}[k]-\boldsymbol{b}_i^\mathrm{H}[k]\,\hat{\boldsymbol{a}}_\mathrm{g}[k]\Big)\mathcal{E}_i^*[k]\,, \quad (33)$$

$$\Gamma_{r_i}[k]=\mathrm{Im}\Big(\mathrm{e}^{-\mathrm{j}\left(\hat{\theta}_{r_i}[k]+\hat{\theta}_{t_1}[k]\right)}\boldsymbol{f}_{1i}^\mathrm{H}[k]\,\boldsymbol{u}_i[k]\,\mathcal{E}_1^*[k] + \mathrm{e}^{-\mathrm{j}\left(\hat{\theta}_{r_i}[k]+\hat{\theta}_{t_2}[k]\right)}\boldsymbol{f}_{2i}^\mathrm{H}[k]\,\boldsymbol{u}_i[k]\,\mathcal{E}_2^*[k]\Big). \quad (34)$$

Proof: See Appendix A. ■

By tracking the transmitter and receiver PN processes independently, IPNT can outperform CPNT significantly, especially for HoM schemes that are more vulnerable to PN distortions. We validate this claim through numerical simulations in Section V.

The adaptive DFE schemes presented in this section, that employ CPNT or IPNT for PN compensation, equalize the combined ISI due to FTN and multipath reflections. While the ISI induced by the multipath propagation is a-priori unknown, the FTN-ISI stemming from the transmitter pulse-shape and the receiver matched-filter is perfectly known at the transmitters and receivers of both polarizations. Therefore, as an alternative to a combined ISI equalization, a separate static equalizer or pre-equalizer can be employed for FTN-ISI mitigation. In the following, we extend the LPE strategy proposed in [44] to the DP-FTN transmission under consideration.

We note that the additive noise samples at the input to the adaptive DFE-CPNT or DFE-IPNT presented in Section III are colored due to FTN signaling [8]. While the LMS filter tap adaptation algorithm remains the same under colored noise [52], [53], the LMS convergence speed may change compared to the white noise scenario due to the increased eigenvalue spread of the auto-correlation matrix of the equalizer inputs [52]–[54]. In fact, [52] shows that the LMS algorithm under colored noise exhibits a directionality of convergence, and hence, the speed of convergence with colored noise can be faster or slower than that with white noise, depending on the initialization of the filter tap weights.

This article has been accepted for publication in a future issue of this journal, but has not been fully edited. Content may change prior to final publication. Citation information: DOI 10.1109/TCOMM.2018.2854164, IEEE Transactions on Communications

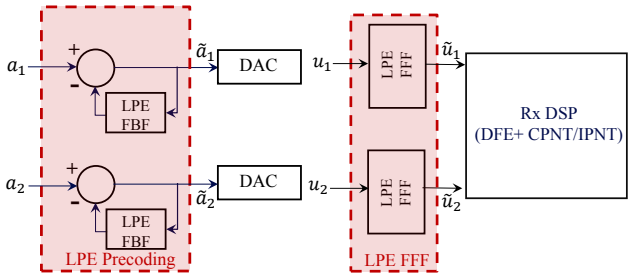

(a) Transmitter (b) Receiver

Fig. 6. LPE-FTN DSP, where the shaded blocks represent additional signal processing compared to a DFE-FTN system.

Moreover, the steady-state MSE with colored noise can also be either larger or smaller than that with white noise [53]. To this end, we finally note that one attractive choice in the existing literature to counter the effects of colored noise due to an FTN transmission is to employ a noise whitening filter (WF) at the receiver [22], [55]. This can also be accomplished through LPE [44], which uses a static FFF at the receiver to whiten the colored noise samples induced by FTN. This serves as an additional motivation to employ LPE in the considered DP-FTN HoM transmission.

IV. XPIC with Precoded FTN

Pre-equalization of the known FTN-ISI can be performed through linear or non-linear precoding at the transmitter [44], [56]–[58]. Since non-linear pre-equalization such as Tomlinson-Harashima precoding [59], [60] can exhibit significant power-loss in an FTN system [44], we focus on linear precoding schemes. We consider the LPE method presented in [44] in the context of an SP transmission and apply it to the DP system considered here to pre-compensate for the FTN-ISI[2]. While LPE by itself is not a novel technique, in the context of a DP-FTN HoM system, it has the following differences compared to [44]: (a) the inputs to the LPE-FFF at the DP receiver are corrupted with multi-path ISI, XPI and PN, and (b) LPE-FBF and LPE-FFF are used *in conjunction* with the DFE-CPNT and DFE-IPNT proposed in Section III of our paper, which constitutes a combined equalizer and PN cancellation structure for the DP transmission. As later shown in Section V-C, this combined structure not only works efficiently, but also outperforms the DFE-only equalization scheme by significant SNR margins.

Fig. 6 illustrates the additional signal processing performed at the transmitter and receiver of a DP LPE-FTN system compared to an unprecoded transmission. At the LPE transmitter of Fig. 6(a), each of the modulated data symbols a_1 and a_2 is filtered by a static LPE-FBF b^{LPE} to produce the sequences $\tilde{a}_1$ and $\tilde{a}_2$, respectively, before the digital-to-analog conversion and pulse-shaping. Similarly, at the LPE receiver shown in Fig. 6(b), the received symbols u_i, $i=1,2$, are filtered by the static LPE-FFF f^{LPE} to generate the sequences $\tilde{u}_i$. Thereafter, the samples $\tilde{u}_i$, $i=1,2$, are processed by the adaptive 2-D DFE to combat the residual interference and PN.

Since the FTN-ISI is perfectly known at the transmitters and receivers for a given pair of β and τ, the filters b^{LPE} and f^{LPE} can be computed in advance, without any feedback from the receivers. In addition to converting the effective FTN-ISI into a minimum-phase impulse response, f^{LPE} also serves the purpose of whitening the noise samples [44], [50] at the 2-D DFE input. The computational details of the LPE-FBF and LPE-FFF are relegated to Appendix B.

Following the LPE-FFF stage at the receiver, the ISI induced by FTN is completely eliminated for each polarization. The residual effects of the multipath ISI, XPI and PN can be subsequently compensated by the LMS-DFE with CPNT or IPNT method. Numerical results presented in the following section show that the combination of LPE precoding and an adaptive 2-D DFE at the receiver outperforms a DFE-only equalization approach. However, as mentioned earlier, LPE-FTN modifies the spectral shape [44].

Finally, we remark that for the FTN equalization methods proposed in Sections III and IV in this paper, we consider DFE and linear precoding, which rely on the spectral factorization [44], [50] of the overall FTN-ISI channel, stemming from the transmitter pulse-shape and the receiver matched filter. When $\tau < \frac{1}{1+\beta}$, the presence of uncountably many spectral zeros makes such factorization unrealizable [44]. Therefore, similar to [44], [56], [57], for our current work, we assume the following relation between β and τ:

$$\tau \geq \frac{1}{1+\beta}\,. \tag{35}$$

While this restriction limits τ to be slightly above the *Mazo limit* [2], [3] corresponding to the same minimum-distance for a given β, the limiting value $\tau = \frac{1}{1+\beta}$ by itself is significantly meaningful as this choice of τ maximizes the FTN capacity [61].

V. Numerical Results and Discussion

In this section, we illustrate and validate the proposed methods by way of numerical simulations. Due to absence of previous works on DP-FTN HoM systems, we benchmark the error-rate performances of the proposed methods against Nyquist transmissions in the presence and absence of PN distortions.

A. Simulation Setup

For the simulations, we consider the discrete-time baseband DP-FTN HoM microwave communication system shown in Fig. 2. FEC coding, modulation and FTN parameters for both polarization branches are kept identical for evaluating the average performance of the DP system. For our simulations, we use a low-density parity-check (LDPC) code[3] with rate 0.9 and codeword length 64800 bits, a random bit-interleaver, 256,

[2]We note that LPE FTN transmission corresponds to a spectral shape modification and thus, it can also be interpreted as using a spectrally more efficient pulse shape [44].

[3]The code is compliant with the second generation digital video broadcasting standard for satellite (DVB-S2) applications [62], [63], and this is encoded as an irregular repeat accumulate (IRA) code. LDPC decoding is performed by iterative standard message passing algorithm [63], with the maximum number of LDPC internal iterations set to 50.

This article has been accepted for publication in a future issue of this journal, but has not been fully edited. Content may change prior to final publication. Citation information: DOI 10.1109/TCOMM.2018.2854164, IEEE Transactions on Communications

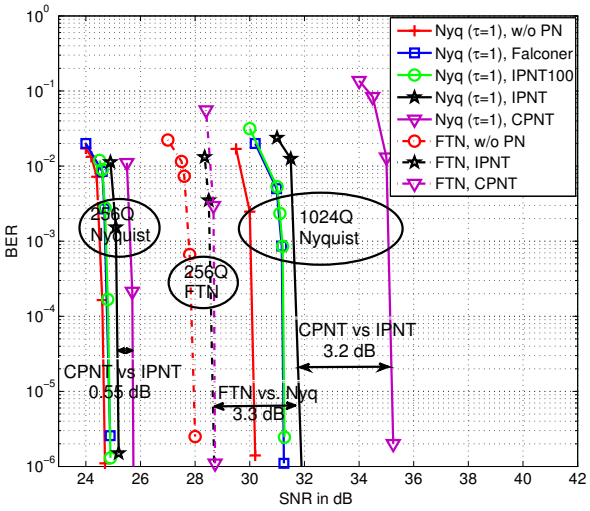

Fig. 7. BER vs. SNR for DP-Nyquist and DP-FTN systems, illustrating the performance gains of DFE-IPNT over DFE-CPNT, and 256-QAM FTN gains over 1024-QAM Nyquist transmission, respectively. $\beta=0.4$, $\tau=1$ (Nyquist) and $\tau=0.8$ (FTN).

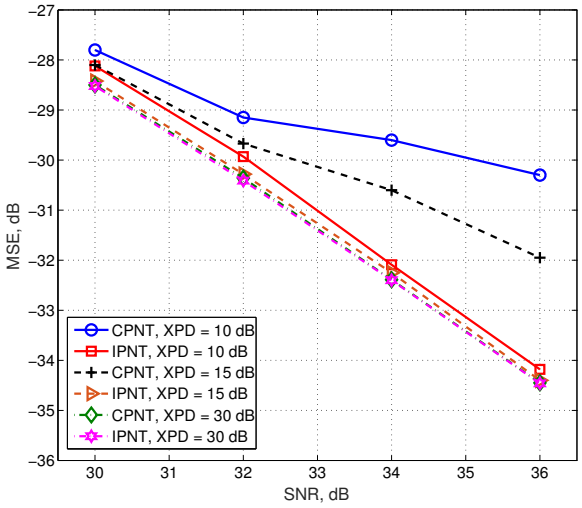

Fig. 8. MSE vs. SNR for 1024-QAM DP-Nyquist systems, illustrating the gains of DFE-IPNT over DFE-CPNT for different XPD values. $\beta=0.4$, $\tau=1$ (Nyquist).

512 and 1024-QAM formats, and different FTN acceleration factors τ for the DP-FTN transmissions. As the roll-off factors of the RRC filters in practical microwave systems can generally vary from 0.25 [12] to 0.5 [11], [14], [64], we have chosen $\beta=0.25$, 0.3 and 0.4 for presenting our results. We consider a 23 Mbaud Nyquist symbol rate for each polarization, which is effectively $\frac{23}{\tau}$ Mbaud with FTN signaling for the same bandwidth [8].

To simulate the Wiener PN processes, we have considered equal contributions of PN due to the transmitter and receiver LOs, such that $\sigma_{w_{t_i}}=\sigma_{w_{r_i}}$, and $\sigma_\Delta=\sqrt{\sigma^2_{w_{t_i}}+\sigma^2_{w_{r_i}}}=0.13^\circ$ [17], [18], $i=1,2$, corresponding to a PN level of -95 dBc/Hz at 100 kHz offset from the center frequency for a 23 Mbaud symbol rate as in [19], [46].

The multipath reflections and XPI, which are assumed to be *unknown* to the transmitters and receivers, are simulated as a 2×2 ISI channel matrix similar to [14]. The matrix elements are modeled by Rummler's well-known fixed-delay, two-ray model [20], such that the frequency response of each element of the channel matrix can be written as a function of frequency f as

$$S_{ij}(f)=a_{ij}\left[1-10^{-\frac{d_{\mathrm{N},ij}}{20}}\mathrm{e}^{\mathrm{j}2\pi(f-f_{\mathrm{N},ij})\tau_0}\right],\, i,j\in\{1,2\}. \quad (36)$$

In (36), $d_{\mathrm{N},ij}$ is the notch-depth set to 5 dB and 3 dB for $i=j$ and $i\neq j$, respectively, $f_{\mathrm{N},ij}$ is the notch-frequency set to 10 MHz and 7 MHz for $i=j$ and $i\neq j$, respectively, $\tau_0=6.3$ ns is a fixed-delay, and a_{ij} is a gain constant normalized to produce unit energy co-polarization channels when $i=j$ and a 15 dB attenuation for $i\neq j$, such that the DP-system has a 15 dB cross-polarization discrimination (XPD) value as in [13], [19].

We consider a 15-tap FFF and a 11-tap FBF for the adaptive DFE. An initial amount of pilot symbols are inserted at the beginning of transmission to ensure LMS convergence, during which the adjustable filter tap-coefficients converge to nearly stationary values as in [41], [49]. Thereafter, four quarternary phase-shift keying (QPSK) training symbols, with the same average power as the data symbols, are transmitted after every 200 data symbols for each polarization, causing a 2% pilot-transmission overhead [17]. The adaptive LMS-DFE switches between training and decision-directed modes across the blocks of pilots and data transmission, respectively. Similar to [41], the step-size parameters associated with the DFE filter tap-weights are chosen to be smaller than those of the PN-estimators to account for faster time-variation of carrier phases over the multipath channel, and their values, together with the decision delay k_0, are optimized to minimize the steady-state MSE. For the DP LPE-FTN system, additional static FBFs and FFFs with 12 and 15 taps, respectively, are applied at the transmitters and receivers of both polarizations as described in Section IV. Following equalization and PN mitigation, soft-demapping is performed on the DFE-outputs and the log-likelihood ratios (LLRs) are passed on to the LDPC decoder.

For the subsequent performance analyses in this section, we consider the DP-Nyquist and the DP-FTN transmissions with the same average transmit power. The error-rate simulations and the SEs of different systems are evaluated as a function of SNR, which for the i^{th} polarization data stream, $i=1,2$, is computed from (3) as

$$\mathrm{SNR}=\frac{\mathbb{E}(|s_i[k]|^2)}{\sigma^2_{n_i}}\,, \quad (37)$$

where $\mathbb{E}(\cdot)$ denotes the expectation operator and s_i is the signal component of the received samples u_i in (3), $i=1,2$, such that

$$s_i[k]=\mathrm{e}^{\mathrm{j}\theta_{r_i}[k]}\sum_{j=1}^{2}\sum_{l}r_j[k-l]\mathrm{e}^{\mathrm{j}\theta_{t_j}[k-l]}h_{ij}[l]\,, \quad (38)$$

This article has been accepted for publication in a future issue of this journal, but has not been fully edited. Content may change prior to final publication. Citation information: DOI 10.1109/TCOMM.2018.2854164, IEEE Transactions on Communications

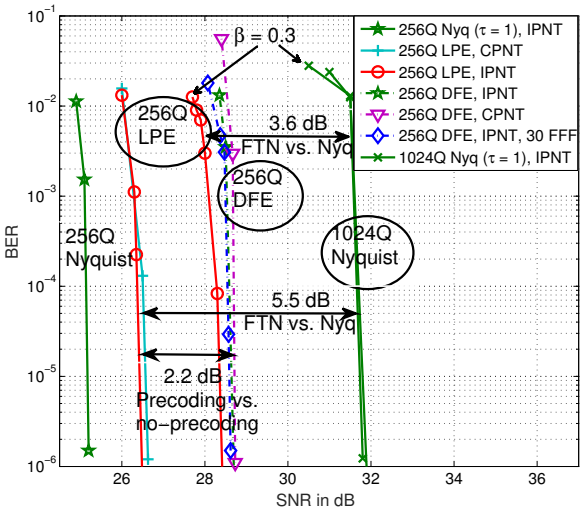

Fig. 9. BER vs. SNR for DP-FTN systems, illustrating the performance gains of LPE-FTN over DFE-FTN. 256 and 1024-QAM, $\beta = 0.3, 0.4$, $\tau = 1$ (Nyquist) and $\tau = 0.8$ (FTN).

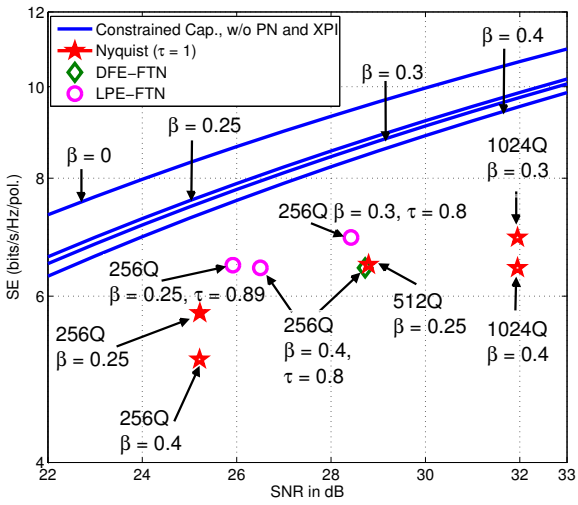

Fig. 10. Spectral efficiency vs. SNR for DP-Nyquist and DP-FTN schemes. 256, 512 and 1024-QAM, $\beta = 0.25, 0.3$ and 0.4, $\tau = 1$ (Nyquist) and $\tau = 0.8, 0.89$ (FTN).

where the sequences r_j, $j = 1, 2$, correspond to the modulated symbols a_j for the unprecoded systems, and the precoded symbols $\tilde{a}_j$ for the LPE precoded FTN transmissions, respectively.

B. Performance with DFE-FTN

We first investigate the efficiency of the proposed algorithms by conducting the following two performance comparisons: (a) CPNT vs. IPNT method, and (b) DP-Nyquist vs. DP-FTN transmissions. For this, we consider the adaptive DFE with the PN mitigation techniques presented in Section III. Fig. 7 shows the coded bit-error rate (BER) performance measured after the LMS convergence. For the computer simulations, 300 codewords are transmitted in each polarization branch, and the average BER performance of both polarization streams is evaluated. For the plots in Fig. 7, the RRC roll-off factor is set to $\beta = 0.4$, and the DP-FTN transmissions use an FTN acceleration factor $\tau = 0.8$. As a reference, we also include the BER performances for the idealized case that the Nyquist and FTN transmissions are not affected by PN distortions, labeled as 'Nyq (τ=1), w/o PN' and 'FTN, w/o PN', respectively, in the figure. Moreover, we have included another benchmark plot in Fig. 7 that serves as an additional reference. The one with the label "Nyq ($\tau = 1$), Falconer" represents the implementation of the method presented in [41] for an SP communication system having the same multi-path ISI and PN simulation setting described in Section V-A.

A comparison of the DFE-CPNT and DFE-IPNT from Fig. 7 shows that the IPNT method outperforms the CPNT technique by 0.55 dB and 3.2 dB for a Nyquist transmission, employing 256 and 1024-QAM, respectively. This indicates that the IPNT exhibits larger gains over the CPNT, particularly for higher modulation formats. Moreover, for both Nyquist and FTN transmissions with 256-QAM, the performance with the IPNT scheme can be observed in Fig. 7 to be within $\sim$0.5 dB from that of a zero-PN system. However, the performance degradation in the presence of PN increases to 1.75 dB with the 1024-QAM Nyquist transmission due to enhanced vulnerability of higher modulation orders to PN impairments. Additionally, we also notice from Fig. 7 that when the XPI is negligibly small with an XPD value of 100 dB, the adaptive DFE-IPNT method, indicated by the label "Nyq ($\tau = 1$), IPNT100" is able to achieve similar BER performance as that of the SP transmission.

To perform a more comprehensive comparison between the IPNT and CPNT methods, we recall from Section III that the gains of DFE-IPNT over DFE-CPNT increase for higher modulation orders as the XPI grows stronger, i.e. for smaller values of XPD [13], [19]. We verify this claim in Fig. 8 by plotting the steady-state MSE averaged over the two polarization data streams as a function of SNR, for a 1024-QAM DP-Nyquist transmission with varying XPD values. As shown in Fig. 8, both IPNT and CPNT yield similar MSEs for milder XPI when XPD = 30 dB. However, as the cross-talk between the two orthogonal polarizations increases, the MSE for IPNT shows significant improvement over CPNT. When the XPI is severe with XPD = 10 dB, the average MSE with the DFE-IPNT scheme can be seen to be 4 dB lower compared to that of the DFE-CPNT at an SNR of 36 dB.

We now proceed to analyze the performance difference between Nyquist and FTN signaling. For this, we first compare the BER of a 256-QAM Nyquist system with that of a 256-QAM FTN transmission. Fig. 7 shows that employing the same modulation order and the DFE-IPNT method, the DP-FTN system offers a 25% increase in the data rate, corresponding to an FTN acceleration factor 0.8, over the DP-Nyquist system at the price of a 3.5 dB SNR penalty. Additionally, in Fig. 7, we also perform a comparison between a 1024-QAM Nyquist system and a 256-QAM FTN transmission having $\tau = 0.8$, such that both systems achieve the same data rate. For example, with a 23 Mbaud Nyquist symbol rate and a

This article has been accepted for publication in a future issue of this journal, but has not been fully edited. Content may change prior to final publication. Citation information: DOI 10.1109/TCOMM.2018.2854164, IEEE Transactions on Communications

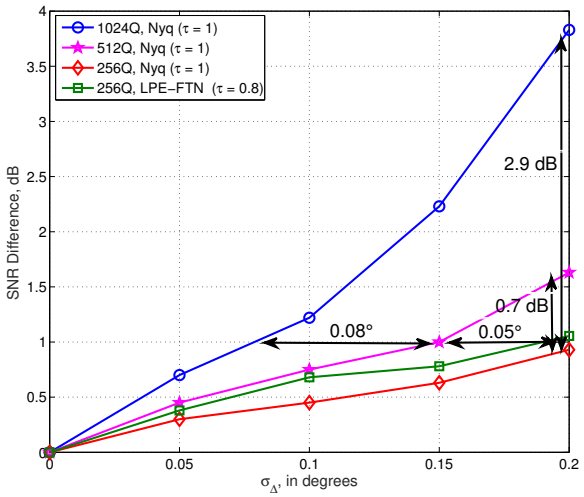

Fig. 11. Additional SNR required over the respective zero-PN reference systems to achieve a BER of 10^{-6}, plotted against σ_Δ. $256, 512, 1024$-QAM, $\beta = 0.4$,$\tau = 1$ (Nyquist) and $\tau = 0.8$ (FTN).

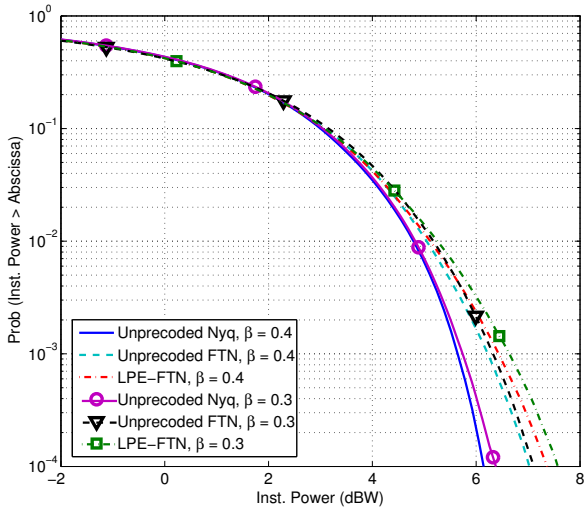

Fig. 12. Empirical CCDF of the instantaneous power with average transmit power = 0 dBW. 256-QAM, $\beta = 0.3$ and 0.4, $\tau = 1$ (Nyquist) and $\tau = 0.8$ (FTN).

LDPC code rate of 0.9, both DP systems employing different modulation schemes yield a data rate of 414 Mbits/sec. Fig. 7 highlights a performance gain of 3.3 dB for the 256-QAM FTN system over the 1024-QAM Nyquist transmission. This suggests that in the presence of PN, with the DFE-IPNT method, a DP-FTN system can significantly outperform a DP-Nyquist transmission that uses a higher modulation format to produce the same data rate.

However, the adaptive DFE described in Section III needs to equalize the combined ISI due to multipath propagation and FTN. As we shall observe in the following, the BER performance of the DP-FTN transmission can be further improved by eliminating the residual FTN-ISI by way of LPE precoding at the transmitter as presented in Section IV.

C. Performance with LPE-FTN

Fig. 9 shows the average BER of the two polarizations for a 256-QAM LPE precoded DP-FTN system with $\tau = 0.8$. Moreover, the RRC roll-off factor is set to $\beta = 0.4$, except for the two plots indicated by the label "$\beta = 0.3$". The figure also includes the Nyquist and DFE-FTN BER curves from Fig. 7 to highlight the gains offered by precoding over unprecoded transmissions. The FTN systems for 256-QAM that employ adaptive DFE to equalize the combined ISI due to multipath and FTN-ISI are labeled by '256Q DFE, CPNT' and '256Q DFE, IPNT'. The precoded DP-FTN systems using LPE for pre-mitigating FTN-ISI are indicated by labels '256Q LPE, CPNT' and '256Q LPE, IPNT'. We observe that the LPE-FTN transmission provides a performance gain of 2.2 dB over the DFE-FTN DP system. For this, LPE uses an additional static FFF at the receiver with 15-taps before the adaptive 15-tap DFE-FFF for each polarization as described in Section IV. For a fair comparison between the precoded and unprecoded systems, we have also plotted the BER of a DFE-FTN transmission that uses 30 taps for the adaptive DFE, labeled '256Q DFE, IPNT, 30 FFF' in Fig. 9, in order to account for the additional LPE filtering at the receiver. However, we note an only marginal improvement with the longer DFE filters. Additionally, Fig. 9 shows 256-QAM LPE-FTN gains of 5.5 dB and 3.6 dB over the 1024-QAM Nyquist systems, with $\beta = 0.4$ and 0.3, respectively. The reduction in gain due to a lower roll-off and the same FTN acceleration factor can be attributed to the stronger FTN-ISI.

The benefits of the DP-FTN HoM systems considered in this paper can be characterized by the SE improvements they provide. The SE value for the i^{th} polarization data stream, $i = 1, 2$, with the RRC roll-off β, FTN factor τ, modulation order M_i, and a code-rate R_i, can be written as

$$\text{SE} = \frac{R_i \log_2(M_i)}{(1+\beta)\tau} \text{ bits/sec/Hz/polarization} . \qquad (39)$$

Fig. 10 shows the SE achieved, per polarization, by the proposed DP-HoM systems as a function SNR, with different values of β and τ. The required SNR to attain a given SE corresponds to an average BER of 10^{-6} for the respective systems. In Fig. 10, we have also included the normalized *constrained capacities* [61] corresponding to different roll-off factors in an SP transmission without PN, as a reference. We note that the normalized capacity with $\beta = 0$ is superior to those of the other RRC pulse-shapes having $\beta > 0$ [61]. As observed from the SE values in the figure, for example, a 256 and a 1024-QAM Nyquist transmission correspond to 5.14 and 6.43 bits/sec/Hz/polarization, respectively, with $\beta = 0.4$, and LDPC code rate 0.9. The SE figures improve with decreasing filter bandwidths as shown for the RRC roll-offs 0.25 and 0.3. We note that by using the FTN factors 0.8 and 0.89, a 256-QAM FTN system can achieve the same SE as a 1024-QAM and a 512-QAM Nyquist transmission, respectively. In Fig. 10, the comparison between the Nyquist and FTN systems that yield the same SE shows that a 256-QAM DP-FTN system with $\tau = 0.8$, using IPNT PN mitigation method and LPE

This article has been accepted for publication in a future issue of this journal, but has not been fully edited. Content may change prior to final publication. Citation information: DOI 10.1109/TCOMM.2018.2854164, IEEE Transactions on Communications

TABLE II
COMPUTATIONAL COMPLEXITIES: CPNT VS. IPNT

Operation	CPNT	IPNT
Complex Addition/Subtraction	$8N_{\mathrm{f}}+4N_{\mathrm{b}}+4=168$	$12N_{\mathrm{f}}+8N_{\mathrm{b}}+16=284$
Complex Multiplication/Division	$12N_{\mathrm{f}}+4N_{\mathrm{b}}+16=240$	$24N_{\mathrm{f}}+8N_{\mathrm{b}}+24=472$
Total Complex Calculations	408	756
Hard Symbol-Decisions	2	2

precoding, can demonstrate a 5.5 dB SNR advantage compared to the 1024-QAM Nyquist system for $\beta = 0.4$. Similarly, a 256-QAM DP LPE-FTN system with $\tau = 0.89$ outperforms a 512-QAM Nyquist system by an SNR margin of 2.9 dB for $\beta = 0.25$. Moreover, the 256-QAM precoded FTN systems with different τ values can be seen to offer a $12-25\%$ higher SE than the 256-QAM Nyquist signaling with a $0.7-3.2$ dB SNR penalty.

Next, we show the PN tolerance of different modulation schemes employing the proposed methods with varying PN intensities. In Fig. 11, we have plotted the additional SNR required over the respective ideal systems that are not affected by PN distortions, to attain a coded BER of 10^{-6}, for each value of σ_{Δ} defined in Section V-A. The figure suggests that lower modulation orders offer higher tolerance to PN distortions. For example, when $\sigma_{\Delta} = 0.2^{\circ}$, 512 and 1024-QAM Nyquist systems show 0.7 dB and 2.9 dB additional SNR penalty from the respective zero-PN reference systems compared to a 256-QAM system. Moreover, at the same SNR distance, e.g. 1 dB from the corresponding zero-PN reference systems, 256-QAM and 512-QAM DP systems tolerate an additional $\sigma_{\Delta} = 1.3^{\circ}$ and 0.08°, respectively, over a 1024-QAM DP-Nyquist transmission, using IPNT PN mitigation method. Furthermore, the PN tolerance of the 256-QAM FTN system is observed to be comparable with that of the 256-QAM Nyquist transmission.

The performance benefits of the LPE precoded FTN systems come at the expense of a possible increase in PAPR. We investigate the PAPR behavior of the precoded and unprecoded 256-QAM FTN systems by plotting the empirical complementary cumulative distribution function (CCDF) of the instantaneous power in Fig. 12. With RRC roll-off 0.3 and 0.4, we also include the PAPR results for the Nyquist transmissions employing 256-QAM for comparison. All transmission schemes are normalized to the same average transmitted power of 0 dBW, such that the 'X-axis' spread to the right hand side of the $X = 0$ dBW line determines the deviation of the peak power from the average power, i.e. PAPR, with the corresponding probability shown along the 'Y-axis'. Fig. 12 suggests that FTN signaling can exhibit a 0.75–0.9 dB higher PAPR than the Nyquist transmission at a CCDF value 10^{-4}. Moreover, PAPR with an FTN transmission increases slightly with smaller RRC roll-off factors as FTN-ISI grows stronger. However, as seen in the figure, the LPE-precoded FTN systems yield only a marginally higher PAPR than the unprecoded FTN transmissions[4].

D. Computational Complexity Analysis

In this section, we present an analysis of the computational cost for the proposed CPNT and IPNT methods. The number of the mathematical operations needed during every symbol period of the DP transmission is furnished in Table II as a function of N_{f} and N_{b}. To illustrate this analysis with further clarity and ease of comparison, a specific example, corresponding to our simulation setting $N_{\mathrm{f}} = 15$ and $N_{\mathrm{b}} = 11$, is also provided. The numbers in Table II reveal that the implementation complexity to update the IPNT estimates according to (23)-(30) is slightly higher than that of the CPNT adaptation given in (7)-(12), at the cost of a significantly superior BER performance demonstrated in Section V-B. Moreover, Table II shows that the LMS adaptation in the decision-directed mode performs two hard symbol decisions for the employed QAM constellation. The table entries also reveal that the number of complex calculations required for the PN and equalizer-taps adaptation does not depend on the modulation order. Therefore, our proposed methods show ease of scalability with higher modulation formats.

VI. Conclusions

A synchronous DP-FTN HoM transmission is an attractive choice to increase the SE in fixed wireless backhaul links. However, the SE improvements offered by such a system comes at the expense of introducing ISI, XPI and vulnerability to PN. Using FTN signaling in a DP transmission can moderate the need for adopting very high modulation orders that are more sensitive to PN distortions. In this paper, DP-FTN HoM systems have been investigated for the first time. In order to equalize interference and recover carrier phase, we proposed a joint XPIC and PN compensation scheme coupled with an adaptive LMS-DFE. The ISI induced by FTN is mitigated either through the LMS-DFE at the receiver or linear pre-equalization at the transmitter. Numerical results for a microwave radio transmission show that an FTN signaling with the proposed interference mitigation schemes can exhibit as high as $3-5.5$ dB performance improvement over a Nyquist transmission that employs a higher modulation order to achieve the same data rate. Alternatively, for a given modulation scheme, a DP-FTN signaling can offer a $12-25\%$ SE enhancement over a DP-Nyquist signaling with a $0.7-3.2$ dB SNR degradation.

[4]We remark that the consideration of PAPR reduction schemes, such as [65] for FTN transmission, and their operation in tandem with pre-distortion methods usually applied for microwave systems using HoM, is an interesting extension to mitigate and analyze the effects of PAPR increase.

This article has been accepted for publication in a future issue of this journal, but has not been fully edited. Content may change prior to final publication. Citation information: DOI 10.1109/TCOMM.2018.2854164, IEEE Transactions on Communications

APPENDIX A
LMS UPDATE EQUATIONS

A. Proof of Lemma 1

To derive the LMS update equations, we rewrite (6) in a more compact way as follows, with the assumption that the PN estimates $\hat{\varphi}_1$ and $\hat{\varphi}_2$ are practically constant over the duration of N_f symbols, corresponding to the FFF length, due to slow PN variation [18], [41], [43]:

$$y_1[k] = \boldsymbol{f}_1^{\mathrm{H}}[k]\,\boldsymbol{P}[k]\boldsymbol{u}_\mathrm{g}[k]-\boldsymbol{b}_1^{\mathrm{H}}[k]\,\hat{\boldsymbol{a}}_\mathrm{g}[k]\,, \tag{40}$$

$$y_2[k] = \boldsymbol{f}_2^{\mathrm{H}}[k]\,\boldsymbol{P}[k]\boldsymbol{u}_\mathrm{g}[k]-\boldsymbol{b}_2^{\mathrm{H}}[k]\,\hat{\boldsymbol{a}}_\mathrm{g}[k]\,. \tag{41}$$

Now, the total MSE over the two polarizations can be written as

$$\mathrm{MSE}_\mathrm{Tot}=\mathbb{E}\big(|\mathcal{E}_1[k]|^2\big)+\mathbb{E}\big(|\mathcal{E}_2[k]|^2\big)\,, \tag{42}$$

where $\mathcal{E}_i[k]=y_i[k]-\hat{a}_i[k-k_0]$ represents the error signal for the i^{th} branch, with $i=1,2$ corresponding to the H and the V-polarization, respectively.

The gradient of $\mathrm{MSE}_\mathrm{Tot}$ with respect to $\boldsymbol{f}_1^*[k]$ follows from (40) and (42) as

$$\frac{\partial\mathrm{MSE}_\mathrm{Tot}}{\partial\boldsymbol{f}_1^*[k]} = \frac{\partial\mathbb{E}\big(|\mathcal{E}_1[k]|^2\big)}{\partial\boldsymbol{f}_1^*[k]} \tag{43}$$

$$= \mathbb{E}\left[\mathcal{E}_1^*[k]\frac{\partial\mathcal{E}_1[k]}{\partial\boldsymbol{f}_1^*[k]}\right] \tag{44}$$

$$= \mathbb{E}\big[\boldsymbol{P}[k]\boldsymbol{u}_\mathrm{g}[k]\mathcal{E}_1^*[k]\big]\,. \tag{45}$$

Similarly, the corresponding gradients of $\mathrm{MSE}_\mathrm{Tot}$ with respect to other filter-tap weights and the PN estimates can be computed as

$$\frac{\partial\mathrm{MSE}_\mathrm{Tot}}{\partial\boldsymbol{f}_2^*[k]} = \mathbb{E}\big[\boldsymbol{P}[k]\boldsymbol{u}_\mathrm{g}[k]\mathcal{E}_2^*[k]\big]\,, \tag{46}$$

$$\frac{\partial\mathrm{MSE}_\mathrm{Tot}}{\partial\boldsymbol{b}_1^*[k]} = -\mathbb{E}\big[\hat{\boldsymbol{a}}_\mathrm{g}[k]\mathcal{E}_1^*[k]\big]\,, \tag{47}$$

$$\frac{\partial\mathrm{MSE}_\mathrm{Tot}}{\partial\boldsymbol{b}_2^*[k]} = -\mathbb{E}\big[\hat{\boldsymbol{a}}_\mathrm{g}[k]\mathcal{E}_2^*[k]\big]\,, \tag{48}$$

$$\frac{\partial\mathrm{MSE}_\mathrm{Tot}}{\partial\hat{\varphi}_1[k]} = 2\mathbb{E}\left[\mathrm{Im}\big(\mathrm{e}^{-\mathrm{j}\hat{\varphi}_1[k]}\psi_1[k]\big)\right]\,, \tag{49}$$

$$\frac{\partial\mathrm{MSE}_\mathrm{Tot}}{\partial\hat{\varphi}_2[k]} = 2\mathbb{E}\left[\mathrm{Im}\big(\mathrm{e}^{-\mathrm{j}\hat{\varphi}_2[k]}\psi_2[k]\big)\right]\,. \tag{50}$$

Now, following the same reasoning as in [41], [49], the minimum MSE with the CPNT method can be achieved by jointly adjusting the tap weights and the PN estimates in proportion to negative values of the respective gradients in (45)-(50). Using the instantaneous values, at a time instant k, as a set of unbiased estimators for the corresponding gradients [51], we get the LMS update equations (7)-(12).

B. Proof of Lemma 2

For the IPNT method, we can rewrite (22) as

$$\tilde{y}_1[k]=\mathrm{e}^{-\mathrm{j}\hat{\theta}_{t_1}[k]}\Big(\boldsymbol{f}_1^{\mathrm{H}}[k]\,\tilde{\boldsymbol{P}}[k]\boldsymbol{u}_\mathrm{g}[k]-\boldsymbol{b}_1^{\mathrm{H}}[k]\,\hat{\boldsymbol{a}}_\mathrm{g}[k]\Big), \tag{51}$$

$$\tilde{y}_2[k]=\mathrm{e}^{-\mathrm{j}\hat{\theta}_{t_2}[k]}\Big(\boldsymbol{f}_2^{\mathrm{H}}[k]\,\tilde{\boldsymbol{P}}[k]\boldsymbol{u}_\mathrm{g}[k]-\boldsymbol{b}_2^{\mathrm{H}}[k]\,\hat{\boldsymbol{a}}_\mathrm{g}[k]\Big). \tag{52}$$

The overall MSE across both polarizations takes the form

$$\mathrm{MSE}_\mathrm{IPNT}=\mathbb{E}\Big(|\tilde{\mathcal{E}}_1[k]|^2\Big)+\mathbb{E}\Big(|\tilde{\mathcal{E}}_2[k]|^2\Big)\,, \tag{53}$$

with $\tilde{\mathcal{E}}_i[k]=\tilde{y}_i[k]-\hat{a}_i[k-k_0]$, $i\in\{1,2\}$. The expressions for the gradients follow as

$$\frac{\partial\mathrm{MSE}_\mathrm{Tot}}{\partial\boldsymbol{f}_1^*[k]} = \mathbb{E}\big[\mathrm{e}^{-\mathrm{j}\hat{\theta}_{t_1}[k]}\tilde{\boldsymbol{P}}[k]\boldsymbol{u}_\mathrm{g}[k]\mathcal{E}_1^*[k]\big]\,, \tag{54}$$

$$\frac{\partial\mathrm{MSE}_\mathrm{Tot}}{\partial\boldsymbol{f}_2^*[k]} = \mathbb{E}\big[\mathrm{e}^{-\mathrm{j}\hat{\theta}_{t_2}[k]}\tilde{\boldsymbol{P}}[k]\boldsymbol{u}_\mathrm{g}[k]\mathcal{E}_2^*[k]\big]\,, \tag{55}$$

$$\frac{\partial\mathrm{MSE}_\mathrm{Tot}}{\partial\boldsymbol{b}_1^*[k]} = -\mathbb{E}\big[\mathrm{e}^{-\mathrm{j}\hat{\theta}_{t_1}[k]}\hat{\boldsymbol{a}}_\mathrm{g}[k]\mathcal{E}_1^*[k]\big]\,, \tag{56}$$

$$\frac{\partial\mathrm{MSE}_\mathrm{Tot}}{\partial\boldsymbol{b}_2^*[k]} = -\mathbb{E}\big[\mathrm{e}^{-\mathrm{j}\hat{\theta}_{t_2}[k]}\hat{\boldsymbol{a}}_\mathrm{g}[k]\mathcal{E}_2^*[k]\big]\,, \tag{57}$$

$$\frac{\partial\mathrm{MSE}_\mathrm{Tot}}{\partial\hat{\theta}_{t_1}[k]} = 2\mathbb{E}\left[\mathrm{Im}\big(\mathrm{e}^{-\mathrm{j}\hat{\theta}_{t_1}[k]}\xi_1[k]\big)\right]\,, \tag{58}$$

$$\frac{\partial\mathrm{MSE}_\mathrm{Tot}}{\partial\hat{\theta}_{t_2}[k]} = 2\mathbb{E}\left[\mathrm{Im}\big(\mathrm{e}^{-\mathrm{j}\hat{\theta}_{t_2}[k]}\xi_2[k]\big)\right]\,, \tag{59}$$

$$\frac{\partial\mathrm{MSE}_\mathrm{Tot}}{\partial\hat{\theta}_{r_1}[k]} = 2\mathbb{E}\big[\Gamma_{r_1}[k]\big]\,, \tag{60}$$

$$\frac{\partial\mathrm{MSE}_\mathrm{Tot}}{\partial\hat{\theta}_{r_2}[k]} = 2\mathbb{E}\big[\Gamma_{r_2}[k]\big]\,. \tag{61}$$

Following a similar argument as in the proof of Lemma 1, (54)-(61) leads to (23)-(30), which completes the proof.

APPENDIX B
LPE-FFF AND LPE-FBF COMPUTATIONS

To derive the expressions for the LPE-FFF and LPE-FBF as in [44], we note that the discrete-time FTN-ISI impulse response for each of the polarization branches can be written as a function of the transmitter pulse-shape and the receiver matched filter as

$$g[n]=(p*q)(n\tau T)\,, \tag{62}$$

where $q(t)=p^*(-t)$ and $*$ denotes the linear convolution.

Introducing $G=\mathcal{Z}\,(g)$, with $\mathcal{Z}(\cdot)$ being the z-transform, we can write the following spectral factorization [50]:

$$G(z)=\lambda V(z)V^*\left(z^{-*}\right)\,, \tag{63}$$

such that $V(z)$ is causal, monic and minimum-phase, and $\lambda>0$ is a scaling factor used to ensure $V(z)$ is monic. As shown in [44], the necessary and sufficient condition for the above spectral factorization is given by

$$\tau\geq\frac{1}{1+\beta}\,. \tag{64}$$

Now, denoting the z-transforms of b^{LPE} and f^{LPE} by $\Psi(z)$ and $\zeta(z)$, respectively, we can write

$$\Psi(z) = V(z)\,, \tag{65}$$

$$\zeta(z) = \frac{1}{\lambda V^*\left(z^{-*}\right)}\,. \tag{66}$$

REFERENCES

[1] M. Jana, L. Lampe, and J. Mitra, "Interference and Phase Noise Mitigation in a Dual-Polarized Faster-than-Nyquist Trasnmission," in *IEEE Int. workshop on Signal Proc. advances in Wireless Commun. (SPAWC)*, 2018.

[2] J. E. Mazo, "Faster-than-Nyquist Signaling," *Bell Syst. Tech. J.*, vol. 54, no. 8, pp. 1451–1462, October 1975.

[3] J. E. Mazo and H. J. Landau, "On the Minimum Distance Problem for Faster-than-Nyquist Signaling," *IEEE Trans. Inf. Theory*, vol. 34, no. 6, pp. 1420–1427, November 1988.

[4] D. Hajela, "On Computing the Minimum Distance for Faster than Nyquist Signaling," *IEEE Trans. Inf. Theory*, vol. 36, no. 2, pp. 289–295, March 1990.

[5] J. B. Anderson, F. Rusek, and V. Owall, "Faster-Than-Nyquist Signaling," in *Proc. IEEE*, vol. 101, no. 8, 2013, pp. 1817–1830.

[6] G. Colavolpe, T. Foggi, A. Modenini, and A. Piemontese, "Faster-than-Nyquist and beyond: how to improve spectral efficiency by accepting interference," *Optics Express*, vol. 19, no. 27, pp. 26 600–26 609, December 2000.

[7] A. D. Liveris and C. N. Georghiades, "Exploiting Faster-than-Nyquist Signaling," *IEEE Trans. Commun.*, vol. 51, no. 9, pp. 1502–1511, September 2003.

[8] F. Rusek, "Partial Response and Faster-than-Nyquist Signaling," Ph.D. dissertation, Lund University, 2007.

[9] P. Noel, M. Prokoptsov, M. Klemes, H. Tai, A. Dufour, and K. Morris, "The Design, Development and Implementation of a Cross-polarization Interference Cancellation System for Point-to-point Digital Microwave Radio systems," in *IEEE Canadian Conf. on Elec. and Comp. Engg. (CCECE)*, 2011.

[10] P. Noel and M. Klemes, "Doubling the Through-Put of a Digital Microwave Radio System by the Implementation of a Cross-Polarization Interference Cancellation Algorithm," in *IEEE Radio and Wireless Symp. (RWS)*, 2012.

[11] B. Lankl, A. Nist, J. A. Nossek, and G. Sebald, "Fully Digital ATDE's and XPIC's for a STM-1 Cochannel Radio System Family," in *IEEE Int. Conf. on Commun. (ICC)*, 1989.

[12] K. W. Suh, C. Y. Park, G. Y. Hur, and D. Y. Lee, "A powerful 13-tap ATDE and XPIC implemented on one chip for co-channel digital radio system," in *IEEE National Telesys. Conf.*, 1994.

[13] H. Proença and N. B. Carvalho, "Cross-Polarization Interference Cancelation (XPIC) Performance in Presence of Non-linear Effects," in *IEEE Workshop on Int. Nonlin. MW and mm-Wave Circ. (INMMIC)*, 2010.

[14] R. Valentin, H. G. Giloi, and K. Metzger, "Performance of Digital Radio Systems in Co-channel Cross-polarized Operation," in *IEEE Global Commun. Conf. (GLOBECOM)*, 1991.

[15] M. Kavehrad, "Baseband Cross-Polarization Interference Cancellation for M-Quadrature AmplitudeModulated Signals Over Multipath Fading Radio Channels," *AT&T Tech. J.*, vol. 64, no. 8, pp. 1913–1926, 1985.

[16] T. Ingason, H. Liu, M. Coldrey, A. Wolfgang, and J. Hansryd, "Impact of Frequency Selective Channels on a Line-of-Sight MIMO Microwave Radio Link," in *IEEE Vehicular Tech. Conf. Spring (VTC)*, 2010.

[17] M. Martalò, G. Ferrari, M. Asim, J. Gambini, C. Mazzucco, G. Cannalire, S. Bianchi, and R. Raheli, "Iterative Synchronization for Dually-Polarized Independent Transmission Streams," *IEEE Trans. Commun.*, vol. 65, no. 6, pp. 2534–2542, 2017.

[18] ——, "Phase noise Compensation for Dually-polarized Systems with Independent Transmission Streams," in *IEEE Int. Symp. on Wireless Commun. Sys. (ISWCS)*, 2015.

[19] A. Vizziello, P. Savazzi, and R. Borra, "Joint Phase Recovery for XPIC System Exploiting Adaptive Kalman Filtering," *IEEE Commn. Lett.*, vol. 20, no. 5, pp. 922–925, 2016.

[20] W. D. Rummler, "A new selective fading model: Application to propagation data," *Bell Syst. Tech. J.*, vol. 58, no. 5, pp. 1037–1071, 1979.

[21] H. Mehrpouyan, A. A. Nasir, S. D. Blostein, T. Eriksson, G. K. Karagiannidis, and T. Svensson, "Joint Estimation of Channel and Oscillator Phase Noise in MIMO Systems," *IEEE Trans. Signal Process.*, vol. 60, no. 9, pp. 4790–4807, 2012.

[22] A. Prlja, J. B. Anderson, and F. Rusek, "Receivers for Faster-than-Nyquist Signaling with and without Turbo Equalization," in *IEEE Int. Symp. on Inf. Theory*, 2008, pp. 464–468.

[23] A. Prlja and J. B. Anderson, "Reduced-Complexity Receivers for Strongly Narrowband Intersymbol Interference Introduced by Faster-than-Nyquist Signaling," *IEEE Trans. Commun.*, vol. 60, no. 9, pp. 2591–2601, September 2012.

[24] F. Rusek and J. B. Anderson, "Successive Interference Cancellation in Multistream Faster-than-Nyquist Signaling," in *Int. Conf. on Wireless Commun. and Mobile Computing*, 2006, pp. 1021–1026.

[25] J. Yu, J. Park, F. Rusek, B. Kudryashov, and I. Bocharova, "High Order Modulation in Faster-Than-Nyquist Signaling Communication Systems," in *IEEE Vehicular Tech. Conf. Fall (VTC)*, 2014.

[26] S. Sugiura, "Frequency-Domain Equalization of Faster-than-Nyquist Signaling," *IEEE Wireless Commun. Lett.*, vol. 2, no. 5, pp. 555–558, October 2013.

[27] S. Sugiura and L. Hanzo, "Frequency-Domain-Equalization-Aided Iterative Detection of Faster-than-Nyquist Signaling," *IEEE Trans. Veh. Technol.*, vol. 64, no. 5, pp. 2122–2128, May 2015.

[28] T. Ishihara and S. Sugiura, "Iterative Frequency-Domain Joint Channel Estimation and Data Detection of Faster-Than-Nyquist Signaling," *IEEE Trans. Wireless Commun.*, vol. 16, no. 9, pp. 6221–6231, 2017.

[29] Q. Shi, N. Wu, X. Ma, and H. Wang, "Frequency-Domain Joint Channel Estimation and Decoding for Faster-Than-Nyquist Signaling," *IEEE Trans. Commun.*, vol. 66, no. 2, pp. 781–795, 2018.

[30] E. Bedeer, M. H. Ahmed, and H. Yanikomeroglu, "Low-Complexity Detection of High-Order QAM Faster-Than-Nyquist Signaling," *IEEE Access*, vol. 5, pp. 14 579–14 588, 2017.

[31] W. Yuan, N. Wu, H. Wang, and J. Kuang, "Variational Inference-Based Frequency-Domain Equalization for Faster-Than-Nyquist Signaling in Doubly Selective Channels," *IEEE Signal Process. Lett.*, vol. 23, no. 9, pp. 1270–1274, 2016.

[32] D. D. Lin, R. A. Pacheco, T. J. Lim, and D. Hatzinakos, "Joint Estimation of Channel Response, Frequency Offset, and Phase Noise in OFDM," *IEEE Trans. Signal Process.*, vol. 54, no. 9, pp. 3542–3554, 2006.

[33] Y. Baeyens, S. Shahramian, B. Jalali, P. Roux, J. Weiner, A. Singh, M. Moretto, P. Boutet, and P. Lopez, "A Wideband SiGe BiCMOS Transceiver Chip-set for High-performance Microwave Links in the 5.643.5 GHz Range," in *IEEE Radio Freq. Int. Circ. Symp. (RFIC)*, 2017.

[34] X. Qi, N. Wu, H. Wang, and W. Yuan, "A Factor Graph-Based Iterative Detection of Faster-than-Nyquist Signaling in the Presence of Phase Noise and Carrier Frequency Offset," *DSP*, vol. 63, pp. 25–34, 2017.

[35] X. Qi, N. Wu, L. Zhou, D. Yang, and H. Wang, "Joint Phase Noise Estimation and Iterative Detection of Faster-than-Nyquist Signaling Based on Factor Graph," in *IEEE Vehicular Tech. Conf. Spring (VTC)*, 2017.

[36] G. Colavolpe, A. Barbieri, and G. Caire, "Algorithms for Iterative Decoding in the Presence of Strong Phase Noise," *IEEE J. Sel. Areas Commun.*, vol. 23, no. 9, pp. 1748–1757, 2005.

[37] A. Barbieri, G. Colavolpe, and G. Caire, "Joint Iterative Detection and Decoding in the Presence of Phase Noise and Frequency Offset," *IEEE Trans. Commun.*, vol. 55, no. 1, pp. 171–179, 2007.

[38] N. Al-Dhahir and A. H. Sayed, "The Finite-Length Multi-Input Multi-Output MMSE-DFE," *IEEE Trans. Signal Process.*, vol. 48, no. 10, pp. 2921–2936, 2000.

[39] R. Merched and N. R. Yousef, "Fast Techniques for Computing Finite-Length MIMO MMSE Decision Feedback Equalizers," *IEEE Trans. Signal Process.*, vol. 54, no. 2, pp. 701–711, 2006.

[40] A. M. Tehrani, B. Hassibi, and J. M. Cioffi, "Adaptive Equalization of Multiple-Input Multiple-Output (MIMO) Channels," in *IEEE Int. Conf. on Commun. (ICC)*, 2000.

[41] D. Falconer, "Application of Passband Decision Feedback Equalization in Two-Dimensional Data Communication Systems," *IEEE Trans. Commun.*, vol. 24, no. 10, pp. 1159–1166, 1976.

[42] S. Moridi and H. Sari, "Analysis of Four Decision-Feedback Carrier Recovery Loops in the Presence of Intersymbol Interference," *IEEE Trans. Commun.*, vol. 33, no. 6, pp. 543–550, 1985.

[43] A. Stark and D. Raphaeli, "Combining Decision-Feedback Equalization and Carrier Recovery for Two-Dimensional Signal Constellations," *IEEE Trans. Commun.*, vol. 55, no. 10, pp. 2012–2021, 2007.

[44] M. Jana, A. Medra, L. Lampe, and J. Mitra, "Pre-equalized Faster-than-Nyquist Transmission," *IEEE Trans. Commun.*, vol. 65, no. 10, pp. 4406–4418, 2017.

[45] A. Demir, A. Mehrotra, and J. Roychowdhury, "Phase noise in Oscillators: A Unifying Theory and Numerical Methods for Characterization," *IEEE Trans. Circuits Syst. I, Fundam. Theory Appl.*, vol. 47, no. 5, pp. 655–674, 2000.

[46] N. Kamiya and E. Sasaki, "Pilot-Symbol Assisted and Code-Aided Phase Error Estimation for High-Order QAM Transmission," *IEEE Trans. Commun.*, vol. 61, no. 10, pp. 4369–4380, 2013.

[47] A. Spalvieri and L. Barletta, "Pilot-Aided Carrier Recovery in the Presence of Phase Noise," *IEEE Trans. Commun.*, vol. 59, no. 7, pp. 1966–1974, 2011.

[48] G. Milotta and A. Carugati, "Communication Between Modems in XPIC Configuration for Wireless Applications ," Patent US8 615 055 B2, 2013. [Online]. Available: http://www.google.com/patents/US8615055

[49] D. D. Falconer, "Jointly adaptive equalization and carrier recovery in two-dimensional digital communication systems," *Bell Syst. Tech. J.*, vol. 55, no. 3, pp. 317–334, 1976.

[50] R. F. H. Fischer, *Precoding and Signal Shaping for Digital Transmission*. Wiley-IEEE Press, 2002.

[51] J. Proakis and M. Salehi, *Digital Communications*. McGraw-Hill Education, 2007.
[52] S. Haykin, *Adaptive Filter Theory*. New Jersy: Prentice-Hall, 1986.
[53] M. Umari, "Effect of Colored Noise on the Performance of LMS Adaptive Equalizers and Predictors," in *IEEE Int. Symp. on Circ. and Sys. (ISCAS)*, 1992.
[54] M. Reuter and J. Zeidler, "Nonlinear Effects in LMS Adaptive Equalizers," *IEEE Trans. Signal Process.*, vol. 47, no. 6, pp. 1570–1579, 1999.
[55] N. Al-Dhahir and J. Cioffi, "MMSE Decision-Feedback Equalizers: Finite-length Results," *IEEE Trans. Inf. Theory*, vol. 41, no. 4, pp. 961–975, 1995.
[56] M. Jana, A. Medra, L. Lampe, and J. Mitra, "Precoded Faster-than-Nyquist Coherent Optical Transmission," in *European Conf. on Opt. Commun. (ECOC)*, 2016.
[57] M. Maso and S. Tomasin, "Pre-equalized Faster Than Nyquist Transmission for 5G Cellular Cicrowave Back-haul," in *IEEE Int. workshop on Signal Proc. advances in Wireless Commun. (SPAWC)*, 2016.
[58] F. Rusek and J. B. Anderson, "Non Binary and Precoded Faster Than Nyquist Signaling," *IEEE Trans. Commun.*, vol. 56, no. 5, pp. 808–817, May 2008.
[59] M. Tomlinson, "New Automatic Equaliser Employing Modulo Arithmetic," *Electronics Letters*, vol. 7, no. 5, pp. 138–139, March 1971.
[60] H. Harashima and H. Miyakawa, "Matched-Transmission Technique for Channels with Intersymbol Interference," *IEEE Trans. Commun.*, vol. 20, no. 4, pp. 774–780, August 1972.
[61] F. Rusek and J. B. Anderson, "Constrained Capacities for Faster-Than-Nyquist Signaling," *IEEE Trans. Inf. Theory*, vol. 55, no. 2, pp. 764–775, February 2009.
[62] *Digital Video Broadcasting (DVB); Second generation framing structure, channel coding and modulation systems for Broadcasting, Interactive Services, News Gathering and other broadband satellite applications (DVB-S2)*, ETSI EN 302 307 V1.2.1 Std. [Online]. Available: www.dvb.org/standards/dvb-s2
[63] H. Ge, "Investigation of LDPC code in DVB-S2," Master's thesis, Linköping University, Dept. of Electrical Engineering, 2012.
[64] B. Lankl, J. Nossek, and G. Sebald, "Cross-polarization Interference Cancellation in the Presence of Delay Effects," in *IEEE Int. Conf. on Commun. (ICC)*, 1988.
[65] S. Peng, A. Liu, K. Wang, and X. Liang, "PAPR Reduction of Multicarrier Faster-Than-Nyquist Signals With Partial Transmit Sequence," *IEEE Access*, vol. 5, pp. 24 931–24 937, 2017.